

Article

Recycled Tire Fibers Used as Reinforcement for Recycled Polyethylene Composites

Hossein Kazemi , Ali Fazli, Jean Philippe Ira and Denis Rodrigue * 

Department of Chemical Engineering and CERMA, Université Laval, Quebec, QC G1V 0A6, Canada; hossein.kazemi.1@ulaval.ca (H.K.); ali.fazli.1@ulaval.ca (A.F.); jean-philippe.ira.1@ulaval.ca (J.P.I.)

* Correspondence: denis.rodrigue@gch.ulaval.ca

Abstract: This study proposes a simple approach to separate most rubber particles from recycled tire fibers (RTFs) and to determine their rubber content using thermogravimetric analysis (TGA)/calcination. Furthermore, scanning electron microscopy (SEM), energy-dispersive X-ray spectroscopy (EDAX), and Fourier transform infrared spectroscopy (FTIR) analyses are used to investigate the separation process and materials compositions. Afterwards, a series of composites based on recycled post-consumer low-density polyethylene (rLDPE) with clean fiber (CF) and residual ground rubber particles (GR) is prepared at different filler concentrations (0–30%) via extrusion compounding before using compression molding and injection molding for comparison. In all cases, injection molding leads to higher strength and modulus but lower elongation at break. The results show that incorporating 30 wt.% of CF into rLDPE yields a remarkable improvement in tensile strength (15%), tensile modulus (192%) and flexural modulus (142%). On the other hand, the incorporation of up to 30 wt.% of GR results in a reduction in both tensile strength and flexural modulus by 15%, confirming the critical role of the cleaning process for RTF in achieving the best results.

Keywords: recycling; polyethylene; tire fibers; ground tire rubber; injection molding; compression molding



Citation: Kazemi, H.; Fazli, A.; Ira, J.P.; Rodrigue, D. Recycled Tire Fibers Used as Reinforcement for Recycled Polyethylene Composites. *Fibers* **2023**, *11*, 74. <https://doi.org/10.3390/fib11090074>

Academic Editor: Faiz Shaikh

Received: 23 June 2023

Revised: 28 August 2023

Accepted: 29 August 2023

Published: 31 August 2023



Copyright: © 2023 by the authors. Licensee MDPI, Basel, Switzerland. This article is an open access article distributed under the terms and conditions of the Creative Commons Attribution (CC BY) license (<https://creativecommons.org/licenses/by/4.0/>).

1. Introduction

Due to a substantial increase in the number of vehicles around the world, more than 1.2 billion tires are produced each year, resulting in the disposal of a huge amount of used tires in landfills after their end of life, generating significant environmental problems [1,2]. For example, more than 260 million tires were discarded in 2019, and between 1 and 3 billion are currently in landfills in the United States alone. Used tires are not biodegradable and require a large space for disposal. Therefore, the tire recycling industry has grown rapidly as the main solution to manage waste tires [3].

Tires are composed on average of 65% rubber, with 20% steel and 15% textile as reinforcements. The majority of recycled tires are processed to retrieve the crumb rubber using separator screens and other technologies. The recovered crumb rubber can be used to create floor mats or as a filler to make thermoplastic elastomers. The steel can also be easily separated from the other components due to its magnetic properties and reused in the metallurgical industry. However, the mixture of pulverized textile fibers (RTFs) and rubber particles is often burned to generate energy or simply dumped in landfills due to processing difficulties [2,4]. For example, their fluffy texture makes them difficult to handle, and large amounts of rubber particles are still attached to the RTFs, which cannot be easily separated. Nevertheless, due to their high aspect ratio (length-to-diameter, L/D), these fibers should be able to reinforce polymer and produce good quality composites, especially for flexible polymers with low modulus and strength [2,5].

Polyester and Nylon, mainly Nylon 6.6, are the predominant polymers found in RTFs [6,7]. While textile fibers have the lowest content in waste tires, they take up more

landfill space due to their low bulk density and accumulate over time since they are non-biodegradable. The valorization of recycled tire fibers is one of the best solutions to reduce waste and minimize depletion. General uses of RTF can be found in composite soil [8–12], reinforced concrete [13–16], asphalt mixture [17–20], and rubber aerogel [21,22]. However, these applications are not able to meet the demand due to the large amounts of RTF generated.

Another possible application of RTF is its use as a filler/reinforcement in polymer composites. Only a few studies can be found for a limited number of polymer matrices such as recycled high-density polyethylene (rHDPE) [23], ground tire rubber [24], and linear low-density polyethylene (LLDPE) [25]. However, none of them considered the separation of RTF from GTR. The presence of a large amount of rubber particles on the surface of RTF results in a non-uniform filler size distribution and poor adhesion with the matrix, leading to low physico-mechanical properties compared to the unfilled polymer. For instance, a study indicated that incorporating 25% RTF (without prior screening and with considerable amounts of GTR particles) into LLDPE resulted in a 15% reduction in tensile modulus and a 19% decrease in flexural strength [26].

RTF is currently one of the most abundant wastes not being recovered due to several processing hurdles and the presence of high amounts of residual rubber particles. Consequently, limited attention has been given to their reuse. This study introduces a simple approach for cleaning and separating rubber particles from RTF, as well as enabling the determination of the rubber content in both the resulting materials: clean fiber (CF) and residual ground rubber (GR). In the following, CF and GR are used as fillers for recycled LDPE (rLDPE), and their effect on the physical properties is investigated. To prepare the composites, rLDPE is firstly pelletized through melt recycling from waste polyethylene foams (electronics packaging). Then, fillers are added to the rLDPE through extrusion, and the resulting blend is molded using compression molding and injection molding. Finally, the physical properties of the molded samples are characterized.

2. Materials and Methods

2.1. Materials

Post-consumer LDPE foams were collected from solid protective packaging waste (Figure 1a). A mixture of crumb rubber and tire fibers from recycled tires was received from Royal Mat Inc. (Beauceville, QC, Canada) (Figure 1b).

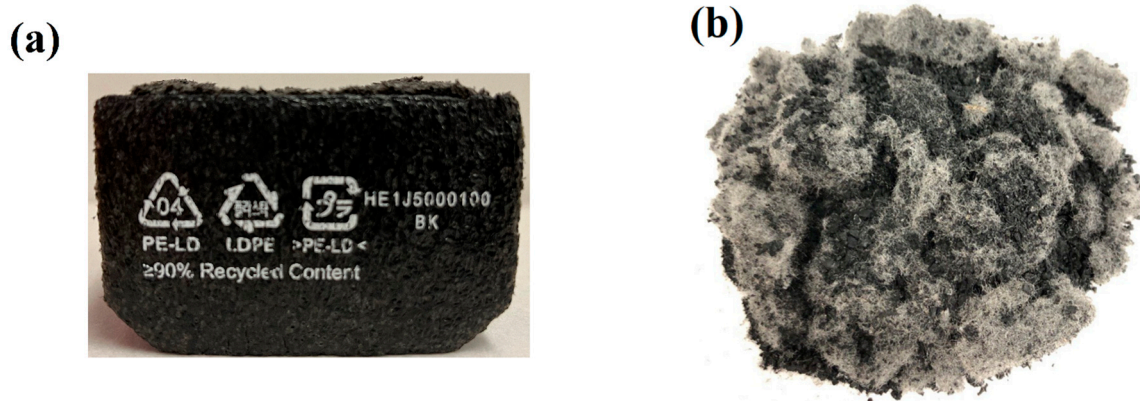


Figure 1. General view of the original materials as received: (a) post-consumer foams and (b) mixture of crumb rubber and tire fibers.

2.2. Tire Fibers Separation

Recycled tire fibers usually contain a large amount of rubber particles of different sizes, which makes it difficult to separate mechanically. Therefore, the mixture of tire fibers and rubber particles was first ground to less than 1 mm using a Retsch cutting mill (Haan, Germany) suitable for reducing the size of materials that do not require extremely high

forces. The feed size is $60 \text{ mm} \times 80 \text{ mm}$, and the rotor speed is 1500 min^{-1} . Then, the ground fibers were sieved with a mesh opening of 1.7 mm . Due to the tendency of tire fibers to entangle and create a felted structure, they form yarns that are larger than 1.7 mm and are retained on the top sieve. Sieved tire fibers are called clean fiber (CF) in this study. On the other hand, rubber particles, which are smaller than 1 mm , pass through the sieve and are collected in the bottom pan. For more separation, the ground rubbers were sieved a second time with a screen mesh size of 46 to isolate particles with a size of $0\text{--}355 \mu\text{m}$. A general view of the resulting materials is shown in Figure 2. It is clear that the color of CF (Figure 2b) is lighter than the original ground tire fibers (Figure 2a) due to sieving out small ground rubber particles. In contrast, the color of GR (Figure 2c) is very dark (black) due to the presence of mainly rubber particles. The average diameter of CF and GR was estimated to be 20 ± 5 and 70 ± 20 microns, respectively, obtained using the Image J 1.53a software (National Institute of Health, Bethesda, Maryland, USA) based on SEM images (Figure 2).

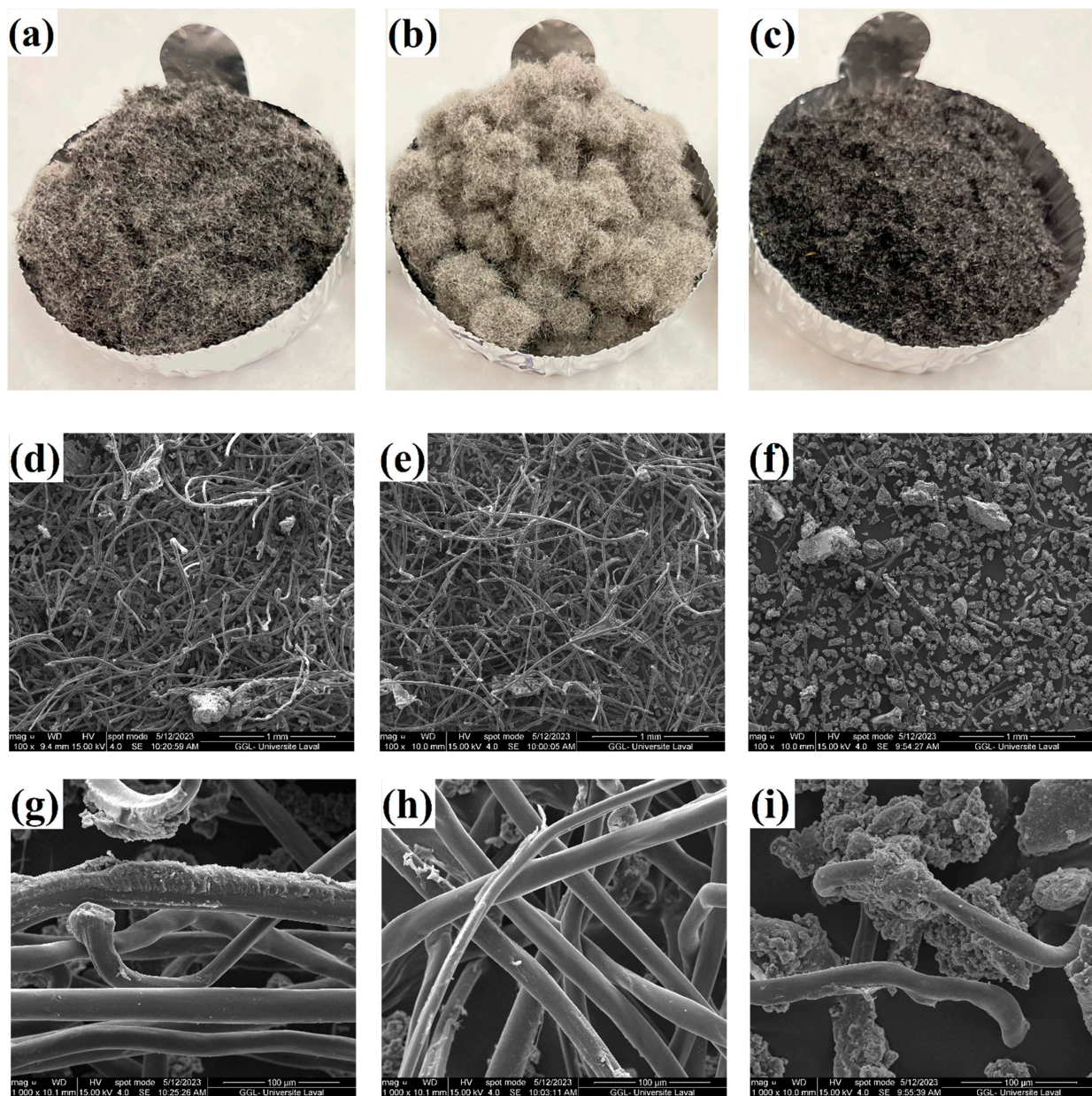


Figure 2. General view and SEM images of the different materials: (a,d,g) ground tire fibers before sieving, (b,e,h) separated CF and (c,f,i) separated GR.

2.3. Polyethylene Foam Recycling

A co-rotating twin-screw extruder Leistritz ZSE-27 with 10 heating zones and a L/D ratio of 40 (die diameter of 2.7 mm) was used for mechanical recycling. The extrusion temperature was set from 130 °C to 150 °C, while the screw speed was set at 50 rpm. The melt was quenched in a water bath and then pelletized using a model 304 pelletizer (Conair, Stanford, CA, USA) to produce rLDPE pellets. All the materials were dried for 24 h in an oven at 70 °C to eliminate any residual water before further processing. A schematic illustration of the recycling process of LDPE foams is shown in Figure 3a.

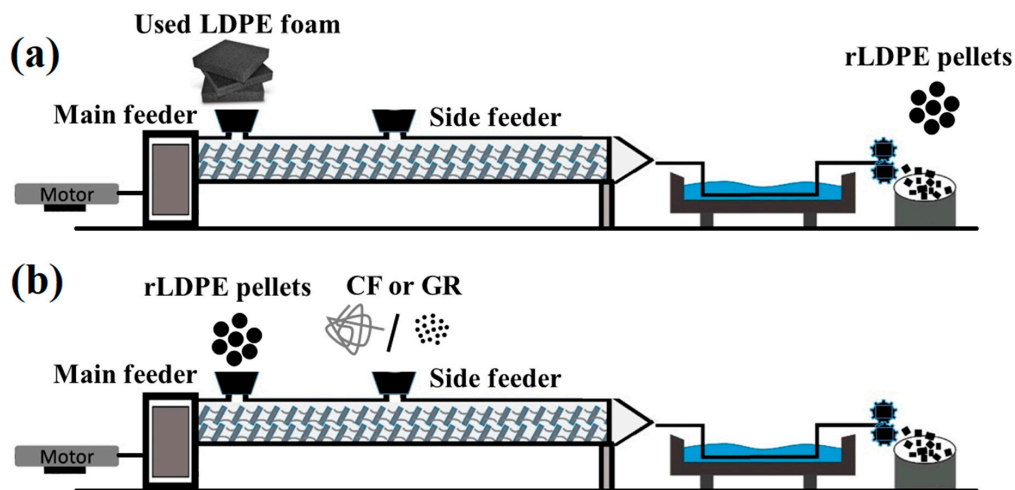


Figure 3. Schematic illustration of: (a) LDPE foams recycling and (b) melt compounding of rLDPE/CF and rLDPE/GR.

2.4. Composite Production

rLDPE composites with different fillers (CF or GR) were produced with the compositions listed in Table 1. The rLDPE pellets were introduced through the main feeder (zone 1), while the fillers (10, 20 and 30 wt.%) were introduced via a side-stuffer located in zone 4 of the extruder to limit thermo-mechanical degradation (Figure 3b). The screw speed for CF and GR was set at 200 rpm and 120 rpm, respectively, while the processing temperature was fixed at 140 °C for both fillers. All the compounds were cooled in a water bath before pelletizing, followed by drying for 24 h in an oven at 70 °C to eliminate any moisture.

Table 1. Coding and compositions of the samples produced.

Sample Code	rLDPE (wt.%)	CF (wt.%)	GR (wt.%)	Molding Method
rLDPE-INJ	100	-	-	Injection
rLDPE-COM	100	-	-	Compression
10CF-INJ	90	10	-	Injection
10CF-COM	90	10	-	Compression
20CF-INJ	80	20	-	Injection
20CF-COM	80	20	-	Compression
30CF-INJ	70	30	-	Injection
30CF-COM	70	30	-	Compression
10GR-INJ	90	-	10	Injection
10GR-COM	90	-	10	Compression
20GR-INJ	80	-	20	Injection
20GR-COM	80	-	20	Compression
30GR-INJ	70	-	30	Injection
30GR-COM	70	-	30	Compression

After drying, the pellets were molded using two different methods: compression molding and injection molding. For injection molding (INJ), a PN60 (Nissei, Japan) Injection molding (IM) was used with an increasing barrel temperature profile at 110–120–130–140 °C (rear, middle, front, and nozzle, respectively) with a mold temperature of 30 °C. The mold has four cavities producing the required shapes directly: two dumbbell forms (type IV as specified by ASTM D638) and two rectangular bars (width and thickness of $12.45 \times 3.14 \text{ mm}^2$ with two lengths of 80 and 125 mm). The samples prepared by injection molding were coded as xCF-INJ and xGR-INJ, where x is the weight filler content and INJ represents the molding process.

Samples were also fabricated via compression molding (COM) using an automatic press (AutoFour/1512-PL,H, 3893, Carver, Wabash, IN, USA). The molding process was carried out at a temperature of 150 °C. The pellets were preheated for 3 min without any pressure, then subjected to 5 min of pressing (force of 3 tons) followed by cooling under pressure to 40 °C using a circulating water system. The mold dimensions were $115 \times 115 \times 3 \text{ mm}^3$, and the specimens were later cut into different geometries for testing. The samples prepared via compression molding were coded as xCF-COM and xGR-COM, where x is the weight filler content and COM represents the molding process.

2.5. Characterizations

2.5.1. Scanning Electron Microscopy (SEM)

The morphology was examined using a FEI Inspect F50 (FEI Company, Hillsboro, OR, USA) scanning electron microscope (SEM). Before analysis, the samples underwent a cryogenic fracture using liquid nitrogen and were then coated with a conductive Pd/Au layer before being imaged at different magnifications.

2.5.2. Fourier Transform Infrared Spectroscopy (FTIR)

Infrared spectra were collected using a Nicolet FTIR spectrometer model 730 (Thermo Fisher Scientific Co., Waltham, MA, USA) with a mercury–cadmium–telluride detector. The characterization was performed using the attenuated total reflection (ATR) method on a diamond crystal. The absorbance was recorded in the range of $4000\text{--}850 \text{ cm}^{-1}$, and each spectrum was an average of 128 scans with a resolution of 4 cm^{-1} .

2.5.3. Thermogravimetric Analysis (TGA)

The thermal stability was studied via thermogravimetric analysis (TGA) using a Q5000 IR (TA Instruments, New Castle, NY, USA). Each test was performed with a heating rate of 10 °C/min from 30 to 750 °C under air.

2.6. Mechanical Properties

2.6.1. Tensile Testing

Tensile properties were determined using a universal testing machine (Instron 5565, Instron, Norwood, OH, USA) based on ASTM D638. Tensile testing was carried out using rectangular specimens with dimensions of $33 \times 6.0 \times 3 \text{ mm}$ and a load cell capacity of 500 N. The specimens were subjected to an extension rate of 10 mm/min , and five replicates were performed for each sample.

2.6.2. Hardness

Hardness (Shore D) was measured using a model 307 L durometer (PTC Instruments, Boston, MA, USA) according to ASTM D2240 with a minimum of five measurements.

2.6.3. Flexural Testing

Flexural tests were carried out on an Instron (Instron, Norwood, OH, USA) model 5565 as per ASTM D790. Rectangular specimens with dimensions of $60 \times 12.7 \times 3 \text{ mm}$ were tested in a three-point bending mode (with a span length of 60 mm) at a speed of 2 mm/min with 5 repetitions conducted for each sample.

3. Results and Discussion

3.1. Characterization of Recycled Materials

Figure 4 shows the FTIR analysis of the materials used. rLDPE exhibits several FTIR absorbance bands, such as at 2915 cm^{-1} , 2850 cm^{-1} and 1460 cm^{-1} , corresponding to aliphatic C-H stretching, symmetric stretching vibration of methyl groups and the bending vibrations of the $-\text{CH}_2-$ groups, respectively. These bands are also observed for virgin LDPE, as reported in the literature [27]. However, an additional band at 1730 cm^{-1} is associated with the stretching vibration of the carbonyl group ($\text{C}=\text{O}$) in an ester functional group that might be found in LDPE foam additives, as well as caused by oxidation or degradation.

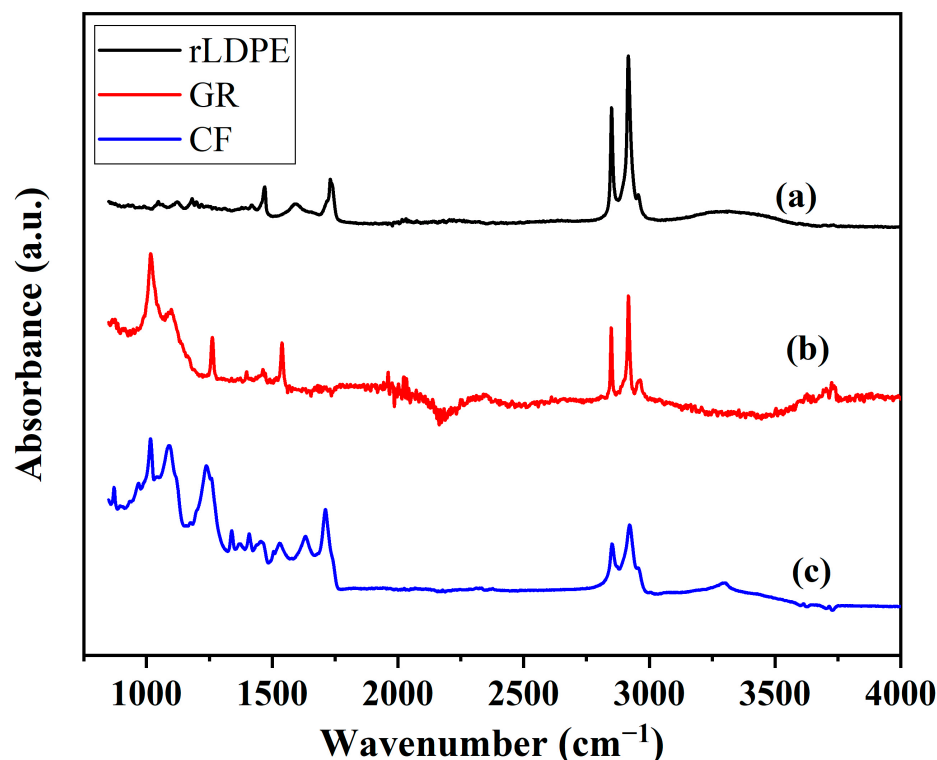


Figure 4. FTIR spectra for: (a) rLDPE, (b) GR and (c) CF.

The FTIR spectrum of GR is complex due to the presence of various compounds. However, the main peaks include the bands in the range of $2920\text{--}2850\text{ cm}^{-1}$, corresponding to stretching vibrations of C-H bonds in the rubber backbone and side chains. Bands located around $1600\text{--}1450\text{ cm}^{-1}$ are associated with the bending vibrations of C-H bonds in aromatic rings and other carbon-based groups. Bands in the $1250\text{--}1000\text{ cm}^{-1}$ region represent the stretching vibrations of C-O and C-N bonds associated with additives used in tire manufacturing. A similar FTIR spectrum was reported for GR by Zedler et al. [28].

Because of the complex CF structure made up of various compounds, its FTIR spectrum is complex to analyze, with multiple peaks representing the different functional groups and chemical bonds in the multicomponent system. For example, the broad band at 3300 cm^{-1} is associated with the stretching vibrations of O-H groups, while the band at 1715 cm^{-1} is associated with the stretching vibrations of C=O bonds in carbonyl groups. Bands located at $1600\text{--}1450\text{ cm}^{-1}$ and $1250\text{--}1000\text{ cm}^{-1}$ represent aromatic rings and the stretching vibrations of C-O bonds. Most of the functional groups found in the CF spectrum are also present in the structure of polyester as the main components of these fibers [25,29]. Previous studies also confirmed the similarity between the FTIR spectrum of RTF and polyester [7,25].

In Figure 5, the energy-dispersive X-ray spectroscopy (EDAX) results for CF and GR are presented. The main elements identified in both CF and GR samples are carbon and

oxygen. However, due to the use of different additives in vulcanized rubber formulations, trace amounts of zinc (Zn), silicon (Si), and sulfur (S) are also detected. A comparison between CF and GR reveals some notable differences. CF exhibits a higher concentration of oxygen compared to GR. This can be attributed to the presence of ester functional groups in polyester, which is the main component of CF.

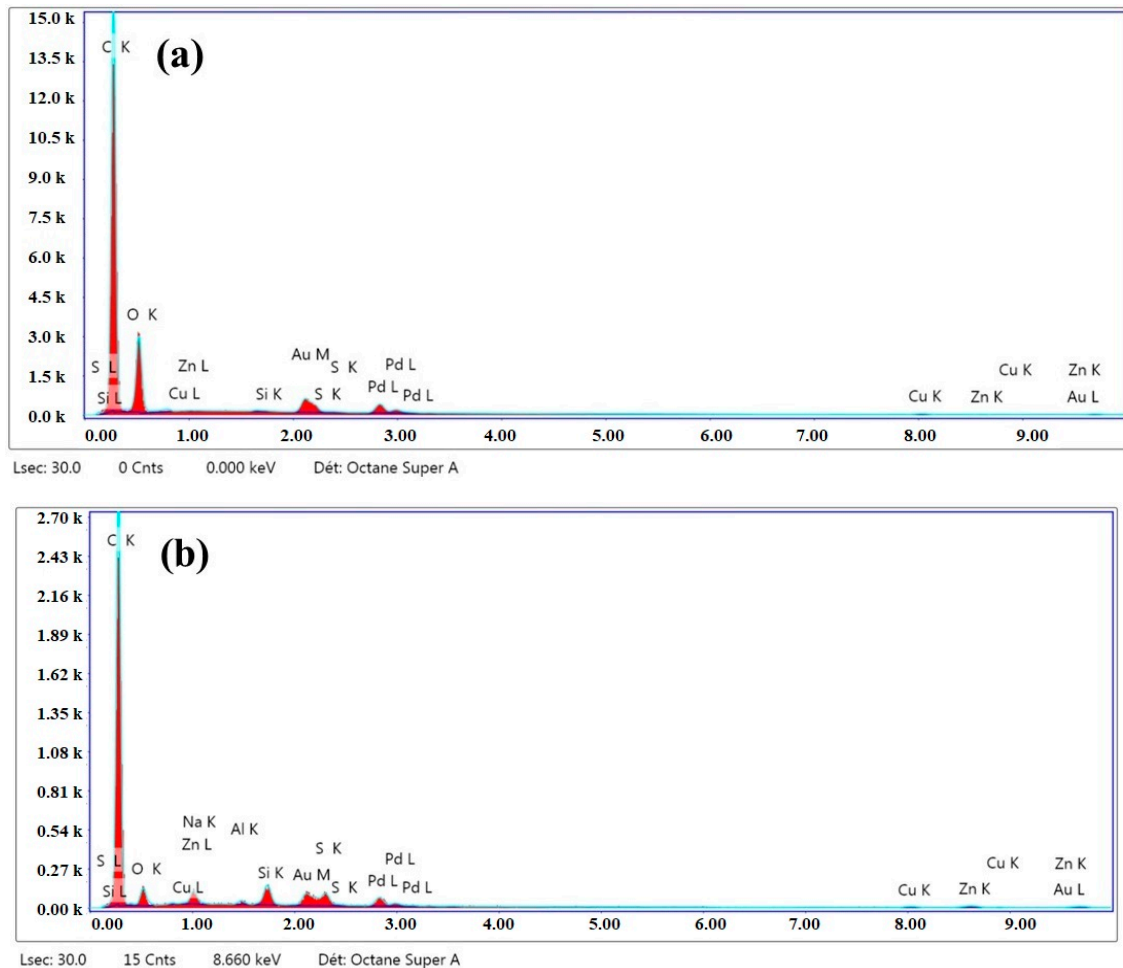


Figure 5. EDAX spectra of: (a) CF and (b) GR.

The elemental compositions of CF and GR are presented in Table 2 in terms of weight and atomic percentage. The results indicate that GR has higher levels of zinc oxide, silicon, and sulfur compared to CF. These elements are typically present in the additives used in vulcanized rubbers and are more prevalent in GR.

Table 2. Chemical analysis compositions of CF and GR (EDAX quantitative results).

Element	CF		GR	
	Weight (%)	Atomic (%)	Weight (%)	Atomic (%)
C	63.26	71.52	83.46	92.46
O	32.41	27.51	5.11	4.24
Si	0.14	0.07	2.05	0.97
S	0.09	0.04	1.87	0.78
Cu	2.50	0.54	2.15	0.45
Zn	1.59	0.33	5.33	1.08

Isolated ground rubber and tire fiber were characterized using TGA to obtain more information on their chemical compositions. For this purpose, several single-crumb rubbers

were collected as isolated ground rubber, while a small skein was carefully separated and washed with water/surfactant solution from the isolated tire fibers to have a minimum amount of rubber content. As shown in Figure 6, the isolated tire fibers completely degrade at 500 °C under air (oxygen) due to their organic nature. On the other hand, around 15 wt.% of crumb rubber is resistant to thermal degradation even at 700 °C. This is due to the presence of inorganic particles, such as silica and calcium carbonate, in the rubber compounds, having high degradation temperatures (above 1000 °C), as well as the high stability of the vulcanized rubber network.

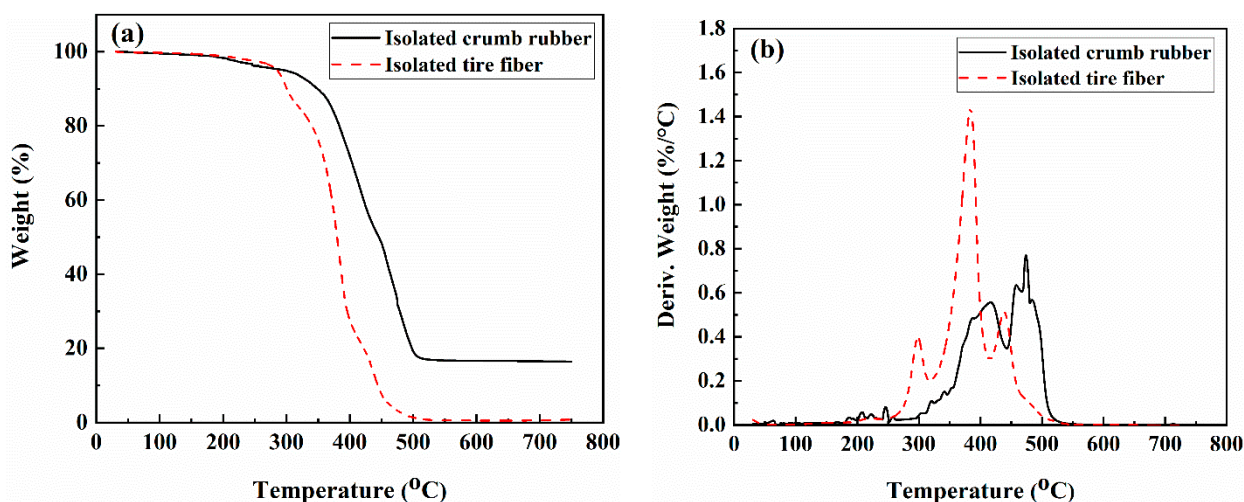


Figure 6. TGA analysis for isolated crumb rubber and isolated tire fiber: (a) weight and (b) derivative weight as a function of temperature.

The difference in the amount of residues (after calcination) for GR and CF can be used to estimate the rubber content. Accordingly, CF and GR were calcinated at 550 °C for 2 h, and the amount of rubber content was estimated as:

$$\text{Rubber content} = \frac{\text{weight loss of sample after calcination} * 100}{\text{weight loss of crumb rubber after calcination} (= 0.15)} \quad (1)$$

The rubber content for the tire fiber, CF and GR was calculated as 66%, 29% and 74%, respectively (Table 3).

Table 3. Rubber content of ground tire fiber, CF and GR after calcination at 550 °C for 2 h, repeated 3 times for each sample.

Sample	Rubber Content (wt.%)
Ground tire fiber	66 ± 2
CF	29 ± 1
GR	74 ± 1

3.2. Morphology

A morphological study of the rLDPE/CF composites is shown in Figure 7. For the composites prepared via injection molding (Figure 7a,b,e,f), the fibers are mostly perpendicular to the cross-section due to the fibers orientation associated with the fountain flow effect in the mold cavity. In fact, injecting the blends directly into a dog-bone-shaped mold caused the specimens to align in the flow direction. On the other hand, the fiber orientation is mainly random for samples prepared via compression molding. There are also more agglomerations (Figure 7c,d,g,h).

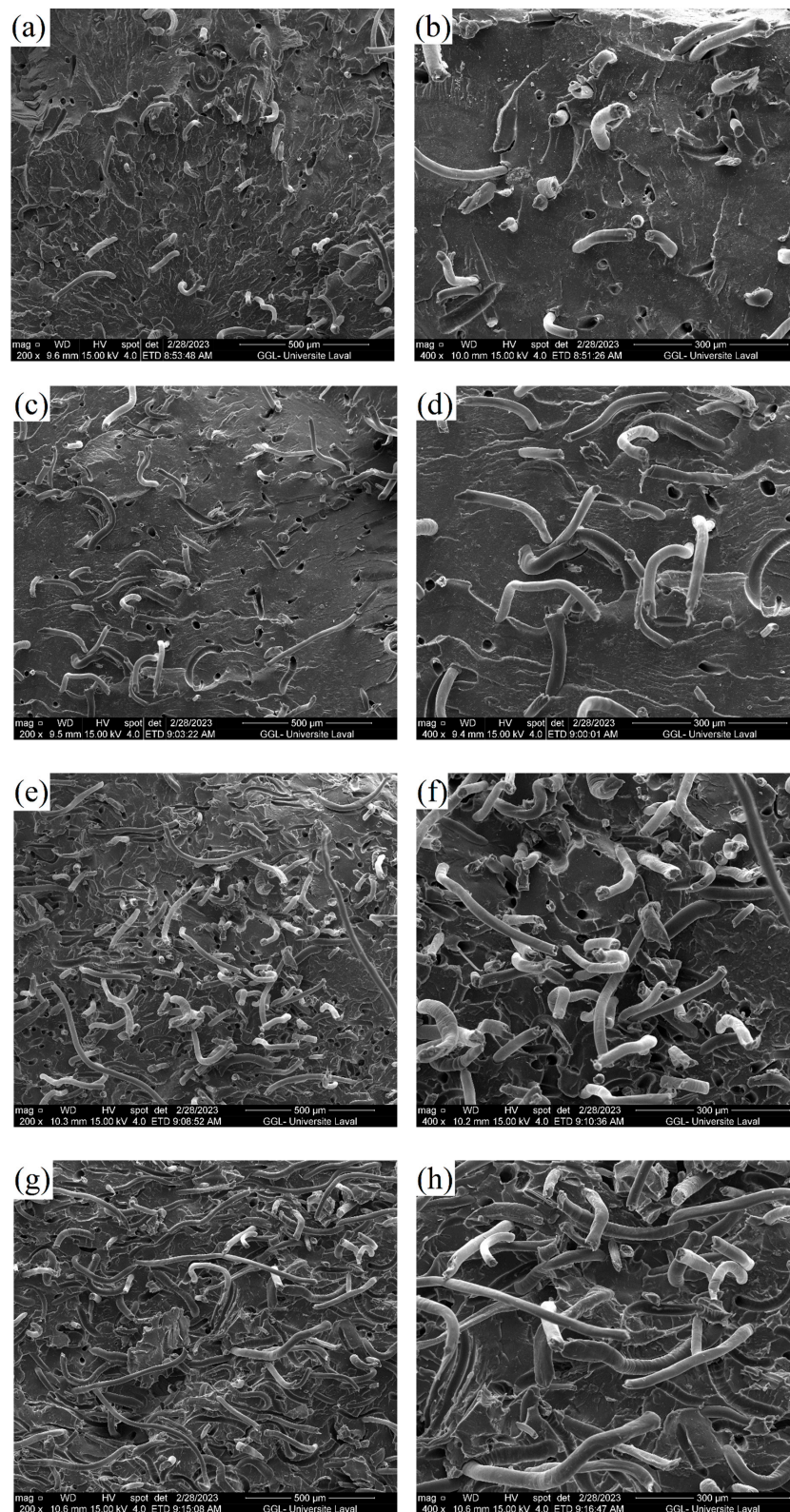


Figure 7. SEM micrographs of rLDPE/CF composites prepared with different molding conditions: 10CF-INJ (a,b), 10CF-COM (c,d), 30CF-INJ (e,f) and 30CF-COM (g,h).

For the compounds filled with GR, better particle dispersion is again observed when injection molding is used compared to compression molding. This is attributed to a

secondary melt-mixing step inside the injection molding screw leading to improved filler dispersion. Typical micrographs of the samples filled with GR are shown in Figure 8.

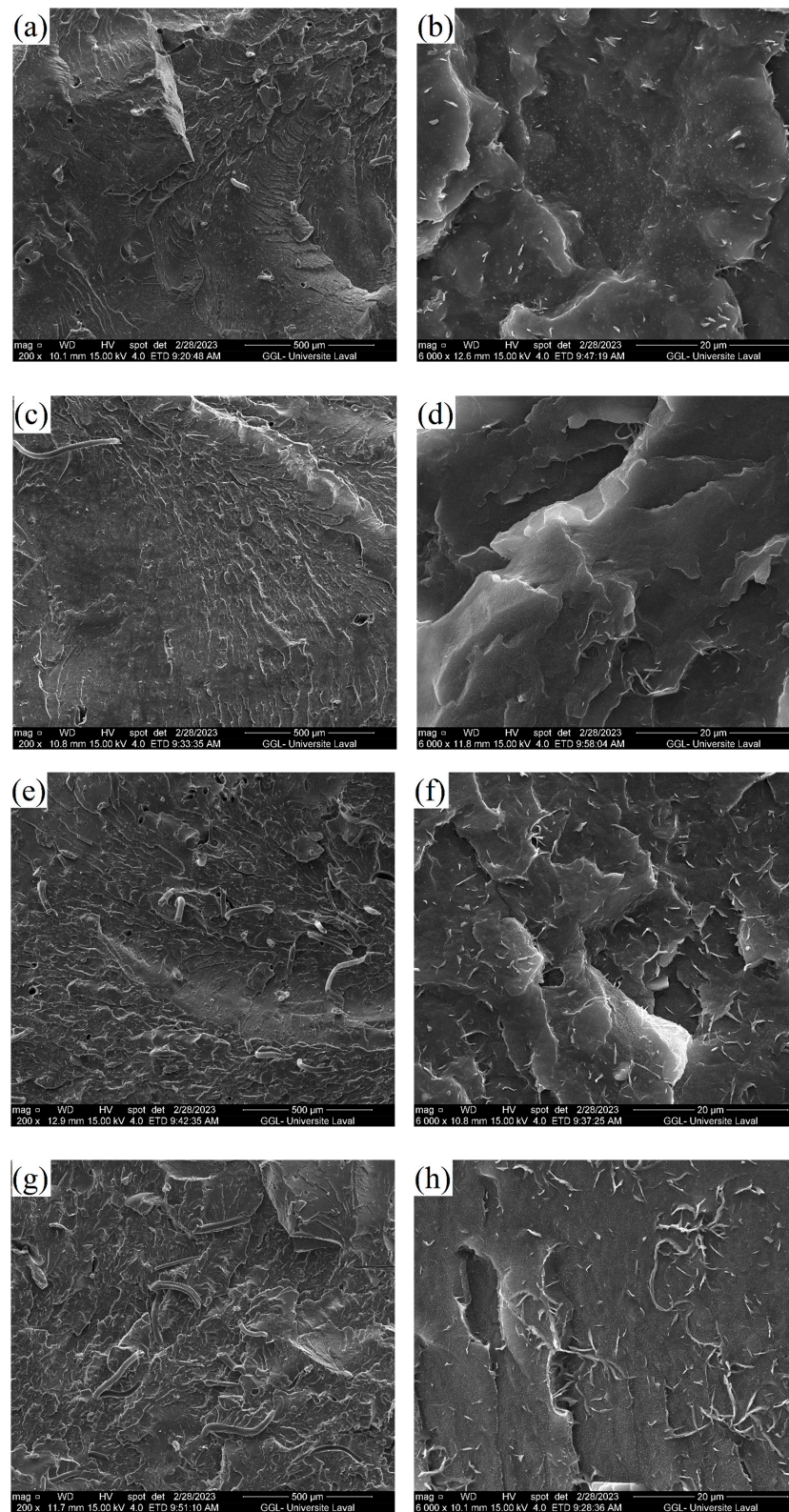


Figure 8. SEM micrographs of rLDPE/GR compounds prepared with different molding conditions: 10GR-INJ (a,b), 10GR-COM (c,d), 30GR-INJ (e,f) and 30GR-COM (g,h).

3.3. Mechanical Properties

Figure 9 shows the effect of filler concentration and molding method on the tensile properties of rLDPE/CF and rLDPE/GR. For all the samples, injection molding leads to higher tensile strength and tensile modulus but lower elongation at break and hardness compared to compression molding. For example, 30CF-INJ has 111% higher tensile strength and 94% higher tensile modulus but 27% lower elongation at break than 30CF-COM. This is ascribed to the secondary melt-mixing step in injection, as well as the orientation of the fibers and polymer chains during injection molding, as reported in the literature [30,31]. Similar observations were obtained from SEM images (Figure 7), indicating that the fibers are mainly oriented perpendicular to the cross-section in injection-molded samples, while the fiber orientation is predominantly random, displaying more entanglements in compression-molded samples.

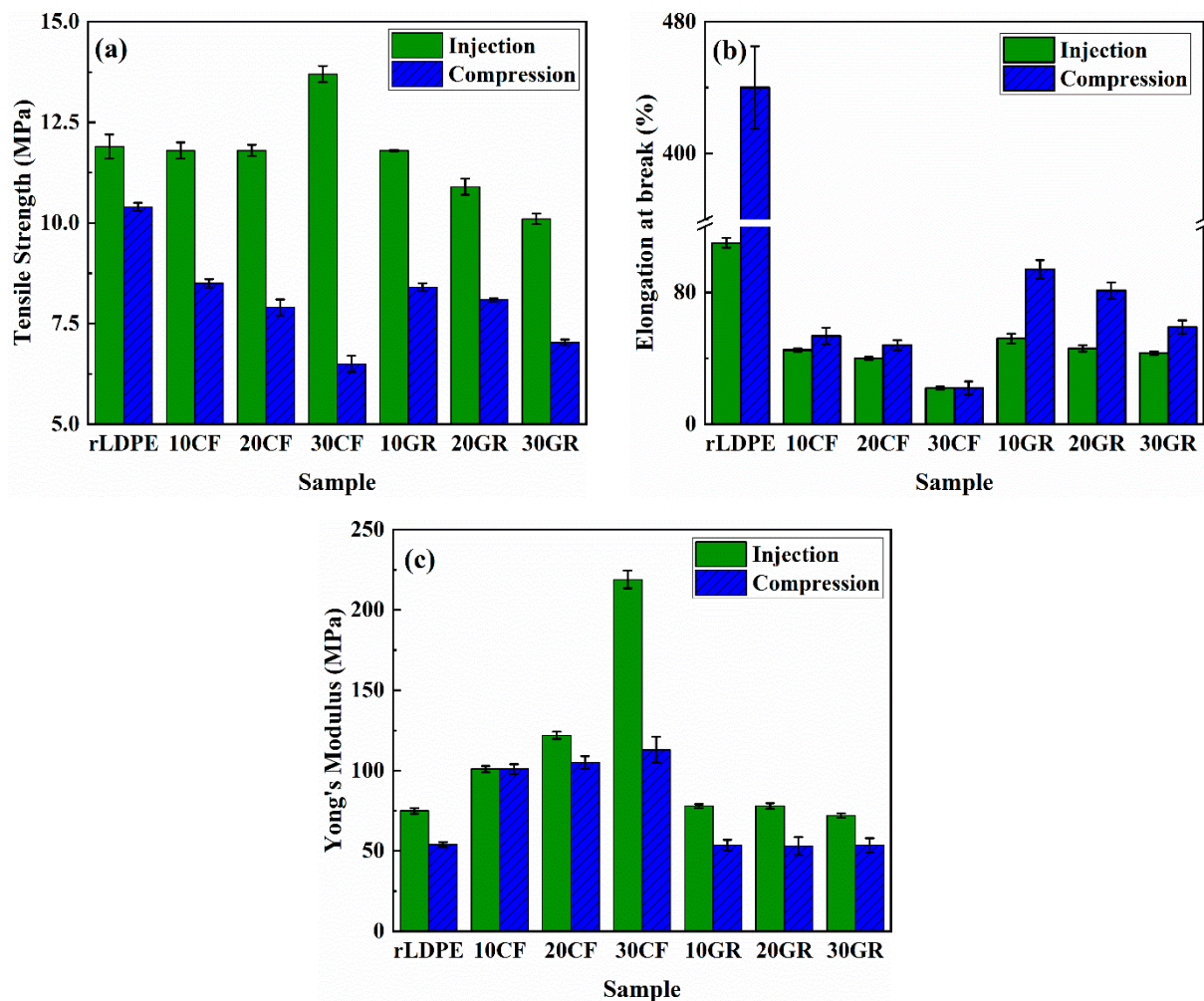


Figure 9. Tensile properties of the rLDPE/CF and rLDPE/GR compounds: (a) tensile strength, (b) elongation at break, and (c) tensile modulus.

A skin–core structure may also be formed during injection molding, as described in the work of Xie et al. [32]. This means that rLDPE polymer chains are elongated in the thin skin due to a shearing effect but also that the fillers/impurities are well embedded in a sample (mostly located in the core). On the other hand, the phase morphology is more isotropic across thickness for compression molded specimens. This theory (morphological difference) supports the results of a higher elongation at break for compression-molded samples compared to injection-molded ones. For example, the elongation at break of

20GR-COM is 76% higher than that of 20GR-INJ. Similar results were observed for HDPE blends in the literature [33,34].

Figure 9 also shows that increasing the CF content from 0 wt.% to 30 wt.% improved the tensile strength and tensile modulus of injection molded composites by 15% (from 11.9 to 13.7 MPa) and 192% (from 75 to 219 MPa), respectively. These improvements are attributed to the high aspect ratio of the CF, creating more filler–filler interactions and entanglements, leading to better resistance to deformation. On the other hand, the presence of tire fibers restricts the mobility of polymer chains, resulting in lower elongation at break. As shown in Figure 9, the elongation at break of injection-molded samples decreased from 45% to 22% with increasing fiber content from 10 wt.% to 30 wt.%.

Regardless of the molding condition, the addition of GR (a soft rubber phase) to rLDPE decreased all tensile properties. This is because of the weak interaction between the crosslinked rubber particles and the matrix (poor compatibility) [35,36]. A higher GR content leads to larger rubber agglomeration with high gel content (crosslinks) acting as stress concentration points at their interface. For instance, 30GR-COM has 37% lower elongation at break and 17% lower tensile strength compared to 10GR-COM. The increased agglomeration among rubber particles is also evident in the morphological analysis (Figure 8) when the GR content increases from 10 wt.% to 30 wt.%.

On the other hand, the tensile modulus does not vary with increasing GR content due to a balance (opposing effect) of the presence of rubber particles and residual tire fibers (Table 3). In fact, the addition of rubber particles decreased the tensile modulus due to its elastic/soft structure, while the presence of tire fibers (more rigid) improves stiffness and strength.

Figure 10a shows the hardness of the composites at different concentrations and processing conditions. Increasing the GR content from 0 to 30 wt.% decreased the hardness from 49.0 to 46.2 Shore D due to the substitution of a more rigid thermoplastic resin with a soft rubber phase. In contrast, the addition of 30 wt.% CF increases the hardness from 49.0 to 53.2 Shore D. In addition, compression-molded samples show slightly higher hardness compared to their injection-molded counterparts. This is because of the secondary melt-mixing step inside the injection molding screw leading to improved filler dispersion and a smoother surface.

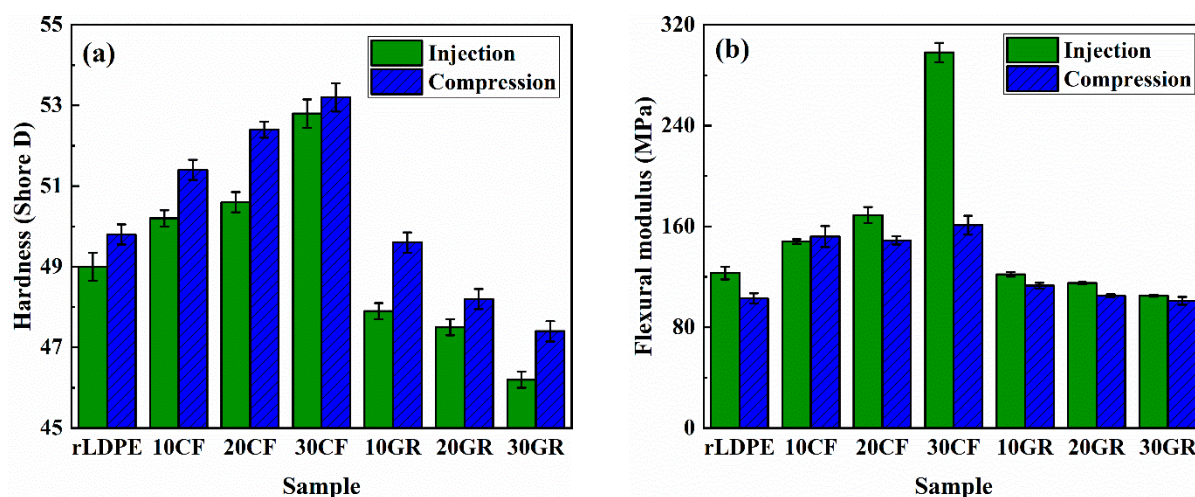


Figure 10. (a) Hardness and (b) flexural modulus of the rLDPE/CF and rLDPE/GR blends.

The flexural modulus of the prepared samples is presented in Figure 10. Similar to the tensile modulus, the flexural modulus showed improvement with the addition of CF, whereas the introduction of GR diminished it. For example, 30CF-INJ has a 142% higher flexural modulus compared to rLDPE-INJ, but the inclusion of 30 wt.% GR decreased the flexural modulus by 15%. Moreover, comparing the compression molding method to injection molding, the latter yields a significantly higher flexural modulus. To illustrate,

the flexural modulus of 30CF-INJ is 85% higher than that of 30CF-COM. This is attributed to the superior dispersion and orientation of fillers in the samples manufactured through injection molding, as depicted in Figure 7.

4. Conclusions

- This study presented a straightforward approach to effectively clean and separate recycled tire fibers (RTFs) from rubber particles to be used as a reinforcement for recycled polyethylene.
- The resulting materials, namely clean fiber (CF) and residual ground rubber (GR), underwent characterization using FTIR, SEM, EDAX, and TGA, providing evidence that the separation process effectively reduced the substantial initial rubber content.
- The findings demonstrated that the incorporation of 30 wt.% of CF into rLDPE (using a combination of extrusion and injection molding) led to a notable improvement in mechanical properties. In particular, a 15% increase in tensile strength with substantial improvements in tensile modulus (192%) and flexural modulus (142%) were achieved.
- Conversely, the addition of GR to rLDPE resulted in a decrease in both tensile strength and flexural modulus by 15%.

Overall, this study proposed the use of clean recycled tire fibers as valuable reinforcement in polymer composites. Therefore, it is recommended to conduct further investigations (such as converting the batch production to a continuous process) into the separation of rubber particles from RTF to enhance efficiency and facilitate industrialization. Additionally, future studies can focus on the applications of finely ground rubber particles as residuals from the RTF cleaning process. Finally, more development must be made to further improve the separation process between RTF and GR.

Author Contributions: Conceptualization, H.K. and D.R.; methodology, H.K., A.F. and J.P.I.; validation, H.K., A.F. and J.P.I.; formal analysis, H.K.; investigation, H.K.; resources, H.K., A.F., J.P.I. and D.R.; data curation, H.K. and D.R.; writing, original draft preparation, H.K.; writing, review and editing, H.K. and D.R.; supervision, D.R.; project administration, D.R.; funding acquisition, D.R. All authors have read and agreed to the published version of the manuscript.

Funding: Financial support was obtained from Royal Mat Inc. (Beauceville, QC, Canada).

Data Availability Statement: Not applicable.

Acknowledgments: The authors gratefully acknowledge Royal Mat Inc (Beauceville, QC, Canada) and RECYC-QUÉBEC for their financial support, as well as the research center on advanced materials (CERMA) for technical support.

Conflicts of Interest: The authors declare no conflict of interest.

References

1. Zainal, S.M.I.S.; Mattius, D.; Baba, Z.; Rizalman, A.N.; Hejazi, F. Improving the Performance of Lightweight Crumb Rubber Mortar Using Synthetic, Natural, and Hybrid Fiber Reinforcements. *Fibers* **2023**, *11*, 9. [\[CrossRef\]](#)
2. Fazli, A.; Rodrigue, D. Sustainable Reuse of Waste Tire Textile Fibers (WTTF) as Reinforcements. *Polymers* **2022**, *14*, 3933. [\[CrossRef\]](#)
3. United States Tire Manufacturers Association. *US Scrap Tire Management Summary*; United States Tire Manufacturers Association: Washington, DC, USA, 2021.
4. Anthony, W.S. Separation of Crumb and Fiber in Tire Recycling Operations. In *ASAE Annual International Meeting*; American Society of Agricultural and Biological Engineers: St. Joseph, MI, USA, 2005.
5. Kazemi, H.; Mighri, F.; Rodrigue, D. A Review of Rubber Biocomposites Reinforced with Lignocellulosic Fillers. *J. Compos. Sci.* **2022**, *6*, 183. [\[CrossRef\]](#)
6. Landi, D.; Gigli, S.; Germani, M.; Marconi, M. Investigating the Feasibility of a Reuse Scenario for Textile Fibres Recovered from End-of-Life Tyres. *Waste Manag.* **2018**, *75*, 187–204. [\[CrossRef\]](#)
7. Onuaguluchi, O.; Banthia, N. Durability Performance of Polymeric Scrap Tire Fibers and Its Reinforced Cement Mortar. *Mater. Struct. Constr.* **2017**, *50*, 1–10. [\[CrossRef\]](#)
8. Abbaspour, M.; Narani, S.S.; Aflaki, E.; Nejad, F.M. Dynamic Characteristics of a Sandy Subgrade Reinforced by Waste Tire Textile Fibres. *Int. J. Pavement Eng.* **2022**, *23*, 2293–2308. [\[CrossRef\]](#)

9. Abbaspour, M.; Narani, S.S.; Aflaki, E.; Nejad, F.M. Behavior of a Subgrade Soil Reinforced by Waste Tire Textile Fibers under Static and Cyclic Loading. *J. Mater. Civ. Eng.* **2020**, *32*, 4020208. [[CrossRef](#)]
10. Reza Tabakouei, A.; Narani, S.S.; Abbaspour, M.; Aflaki, E.; Siddiqua, S. Coupled Specimen and Fiber Dimensions Influence Measurement on the Properties of Fiber-Reinforced Soil. *Meas. J. Int. Meas. Confed.* **2022**, *188*, 110556. [[CrossRef](#)]
11. Valipour, M.; Shourijeh, P.T.; Mohammadinia, A. Application of Recycled Tire Polymer Fibers and Glass Fibers for Clay Reinforcement. *Transp. Geotech.* **2021**, *27*, 100474. [[CrossRef](#)]
12. Abbaspour, M.; Aflaki, E.; Moghadas Nejad, F. Reuse of Waste Tire Textile Fibers as Soil Reinforcement. *J. Clean. Prod.* **2019**, *207*, 1059–1071. [[CrossRef](#)]
13. Gil, L.; Bernat-Masó, E.; Cañavate, F.J. Changes in Properties of Cement and Lime Mortars When Incorporating Fibers from End-of-Life Tires. *Fibers* **2016**, *4*, 7. [[CrossRef](#)]
14. Chen, M.; Zhong, H.; Chen, L.; Zhang, Y.; Zhang, M. Engineering Properties and Sustainability Assessment of Recycled Fibre Reinforced Rubberised Cementitious Composite. *J. Clean. Prod.* **2021**, *278*, 123996. [[CrossRef](#)]
15. Serdar, M.; Baričević, A.; Jelčić Rukavina, M.; Pezer, M.; Bjegović, D.; Štirmer, N. Shrinkage Behaviour of Fibre Reinforced Concrete with Recycled Tyre Polymer Fibres. *Int. J. Polym. Sci.* **2015**, *2015*, 145918. [[CrossRef](#)]
16. Baričević, A.; Jelčić Rukavina, M.; Pezer, M.; Štirmer, N. Influence of Recycled Tire Polymer Fibers on Concrete Properties. *Cem. Concr. Compos.* **2018**, *91*, 29–41. [[CrossRef](#)]
17. Bocci, E.; Prospero, E. Recycling of Reclaimed Fibers from End-of-Life Tires in Hot Mix Asphalt. *J. Traffic Transp. Eng.* **2020**, *7*, 678–687. [[CrossRef](#)]
18. Landi, D.; Marconi, M.; Bocci, E.; Germani, M. Comparative Life Cycle Assessment of Standard, Cellulose-Reinforced and End of Life Tires Fiber-Reinforced Hot Mix Asphalt Mixtures. *J. Clean. Prod.* **2020**, *248*, 119295. [[CrossRef](#)]
19. Jin, D.; Ge, D.; Zhou, X.; You, Z. Asphalt Mixture with Scrap Tire Rubber and Nylon Fiber from Waste Tires: Laboratory Performance and Preliminary M-E Design Analysis. *Buildings* **2022**, *12*, 160. [[CrossRef](#)]
20. Pais, J.C.; Santos, C.R.G.; Lo Presti, D. Application of Textile Fibres from Tire Recycling in Asphalt Mixtures. *Road Mater. Pavement Des.* **2022**, *23*, 2353–2374. [[CrossRef](#)]
21. Thai, Q.B.; Chong, R.O.; Nguyen, P.T.T.; Le, D.K.; Le, P.K.; Phan-Thien, N.; Duong, H.M. Recycling of Waste Tire Fibers into Advanced Aerogels for Thermal Insulation and Sound Absorption Applications. *J. Environ. Chem. Eng.* **2020**, *8*, 104279. [[CrossRef](#)]
22. Ba Thai, Q.; Ee Siang, T.; Khac Le, D.; Shah, W.A.; Phan-Thien, N.; Duong, H.M. Advanced Fabrication and Multi-Properties of Rubber Aerogels from Car Tire Waste. *Colloids Surfaces A Physicochem. Eng. Asp.* **2019**, *577*, 702–708. [[CrossRef](#)]
23. Fazli, A.; Rodrigue, D. Phase Morphology, Mechanical, and Thermal Properties of Fiber-Reinforced Thermoplastic Elastomer: Effects of Blend Composition and Compatibilization. *J. Reinf. Plast. Compos.* **2022**, *41*, 267–283. [[CrossRef](#)] [[PubMed](#)]
24. Zhang, X.X.; Lu, C.H.; Liang, M. Preparation of Rubber Composites from Ground Tire Rubber Reinforced with Waste-Tire Fiber through Mechanical Milling. *J. Appl. Polym. Sci.* **2007**, *103*, 4087–4094. [[CrossRef](#)]
25. Moghaddamzadeh, S.; Rodrigue, D. The Effect of Polyester Recycled Tire Fibers Mixed with Ground Tire Rubber on Polyethylene Composites. Part I: Morphological Analysis. *Prog. Rubber Plast. Recycl. Technol.* **2018**, *34*, 200–220. [[CrossRef](#)]
26. Moghaddamzadeh, S.; Rodrigue, D. The Effect of Polyester Recycled Tire Fibers Mixed with Ground Tire Rubber on Polyethylene Composites. Part II: Physico-Mechanical Analysis. *Prog. Rubber Plast. Recycl. Technol.* **2018**, *34*, 128–142. [[CrossRef](#)]
27. Doğan, Ö.; Karadagli, I. Pyrolysis of Low and High Density Polyethylene. Part II: Analysis of Liquid Products Using FTIR and NMR Spectroscopy. *Energy Sources Part A-Recovery Util. Environ. Eff.* **2008**, *30*, 392–400. [[CrossRef](#)]
28. Zedler, L.; Kowalkowska-Zedler, D.; Colom, X.; Cañavate, J.; Saeb, M.R.; Formela, K. Reactive Sintering of Ground Tire Rubber (GTR) Modified by a Trans-Polyoctenamer Rubber and Curing Additives. *Polymers* **2020**, *12*, 3018. [[CrossRef](#)]
29. Kang, E.; Kim, M.; Oh, J.S.; Park, D.W.; Shim, S.E. Electrospun BMIMPF₆/Nylon 6,6 Nanofiber Chemiresistors as Organic Vapour Sensors. *Macromol. Res.* **2012**, *20*, 372–378. [[CrossRef](#)]
30. Pérez-Fonseca, A.A.; Martín Del Campo, A.S.; Robledo-Ortíz, J.R.; González-López, M.E. Compatibilization Strategies for PLA Biocomposites: A Comparative Study between Extrusion-Injection and Dry Blending-Compression Molding. *Compos. Interfaces* **2022**, *29*, 274–292. [[CrossRef](#)]
31. Scoponi, G.; Francini, N.; Athanassiou, A. Production of Green Star/Linear PLA Blends by Extrusion and Injection Molding: Tailoring Rheological and Mechanical Performances of Conventional PLA. *Macromol. Mater. Eng.* **2021**, *306*, 2000805. [[CrossRef](#)]
32. Xie, M.; Chen, J.; Li, H. Morphology and Mechanical Properties of Injection-Molded Ultrahigh Molecular Weight Polyethylene/polypropylene Blends and Comparison with Compression Molding. *J. Appl. Polym. Sci.* **2009**, *111*, 890–898. [[CrossRef](#)]
33. Yang, H.; Yilmaz, G.; Jiang, J.; Langstraat, T.; Chu, R.; van Es, M.; Garg, P.; Turng, L.S. Thermal, Rheological, and Mechanical Characterization of Compression and Injection Molded Ultra-High Molecular Weight Polyethylene, High Density Polyethylene, and Their Blends. *J. Appl. Polym. Sci.* **2023**, *140*, e53484. [[CrossRef](#)]
34. Mejia, E.; Cherupurakal, N.; Mourad, A.H.I.; Al Hassanieh, S.; Rabia, M. Effect of Processing Techniques on the Microstructure and Mechanical Performance of High-density Polyethylene. *Polymers* **2021**, *13*, 3346. [[CrossRef](#)] [[PubMed](#)]

35. Kiss, L.; Simon, D.Á.; Petrény, R.; Kocsis, D.; Bárány, T.; Mészáros, L. Ground Tire Rubber Filled Low-Density Polyethylene: The Effect of Particle Size. *Adv. Ind. Eng. Polym. Res.* **2022**, *5*, 12–17. [[CrossRef](#)]
36. Colom, X.; Cañavate, J.; Carrillo, F.; Suñol, J.J. Effect of the Particle Size and Acid Pretreatments on Compatibility and Properties of Recycled HOPE Plastic Bottles Filled with Ground Tyre Powder. *J. Appl. Polym. Sci.* **2009**, *112*, 1882–1890. [[CrossRef](#)]

Disclaimer/Publisher’s Note: The statements, opinions and data contained in all publications are solely those of the individual author(s) and contributor(s) and not of MDPI and/or the editor(s). MDPI and/or the editor(s) disclaim responsibility for any injury to people or property resulting from any ideas, methods, instructions or products referred to in the content.